

Millimeter Wave Small-Scale Spatial Statistics in an Urban Microcell Scenario

Shu Sun, Hangsong Yan, George R. MacCartney Jr., and Theodore S. Rappaport
NYU WIRELESS and NYU Tandon School of Engineering, New York University, Brooklyn, NY, USA 11201
{ss7152,hy942,gmac,tsr}@nyu.edu

Abstract—This paper presents outdoor wideband small-scale spatial fading and autocorrelation measurements and results in the 73 GHz millimeter-wave (mmWave) band conducted in downtown Brooklyn, New York. Both directional and omnidirectional receiver (RX) antennas are studied. Two pairs of transmitter (TX) and RX locations were tested with one line-of-sight (LOS) and one non-line-of-sight (NLOS) environment, where a linear track was employed at each RX to move the antenna in half-wavelength increments. Measured data reveal that the small-scale spatial fading of the received signal voltage amplitude are generally Ricean-distributed for both omnidirectional and directional RX antenna patterns under both LOS and NLOS conditions in most cases, except for the log-normal distribution for the omnidirectional RX antenna pattern in the NLOS environment. Sinusoidal exponential and typical exponential functions are found to model small-scale spatial autocorrelation of the received signal voltage amplitude in LOS and NLOS environments in most cases, respectively. Furthermore, different decorrelation distances were observed for different RX track orientations, i.e., for different directions of motion relative to the TX. Results herein are valuable for characterizing small-scale spatial fading and autocorrelation properties in multiple-input multiple-output (MIMO) systems for fifth-generation (5G) mmWave frequencies.

Index Terms—5G, mmWave, MIMO, small scale, fading, autocorrelation.

I. INTRODUCTION

The millimeter-wave (mmWave) bands hold promising prospects for providing substantially broader bandwidths and higher data rates required for the fifth-generation (5G) wireless communications [1]. There have been intensive investigations on mmWave propagation characteristics and channel modeling in various environments [2]–[7], which is paving the way for 5G mmWave system design and deployment. Nevertheless, the knowledge on some aspects of mmWave propagation is still scarce, such as small-scale spatial fading and autocorrelation properties of received signal voltage amplitudes, which are crucial in multiple-input multiple-output (MIMO) channel modeling for 5G wireless communications.

Previously, indoor continuous-wave (CW) propagation experiments and analysis at 910 MHz were performed in [8], which showed that both temporal and spatial signal envelope fading distributions were Ricean with K -factors of 6 dB to 12 dB and 2 dB, respectively [8]. Indoor corridor measurements were conducted to study small-scale fading characteristics at 15 GHz [9], which demonstrated that small-scale fading in indoor corridor scenarios could be well described by Ricean

distributions with K -factors ranging from 5 dB to 10 dB for most measurement locations when omnidirectional antennas were used at both the transmitter and receiver, while the value of Ricean K -factors increased significantly when employing directional antennas. Another measurement campaign carried out in an industrial environment showed the applicability of the Rayleigh distribution for modeling the small-scale fading for all time excess delay bins except the first one that was inclined to be Nakagami- m fading [10], whereas [11] found that log-normal distribution was a better fit over all time bins. The impact of bandwidth on the small-scale fade depth was explored in [12], indicating a decrease in the fade depth as the bandwidth increased, attaining 4 dB fade depth at 1 GHz. For a bandwidth exceeding 1 GHz, the fade depth became less dynamic over bandwidth. The work in [13] and [14] also showed decreased fading depths as the signal bandwidth became larger. Durgin *et al.* [15] noticed that at 1.92 GHz fade depths would decrease when more directional antennas were used. Henderson *et al.* examined a 2.4 GHz indoor channel and tried to find an appropriate small-scale fading distribution [16]. Three types of distributions were utilized to fit the measured data: Rayleigh, Ricean, and Two-Wave-Diffuse-Power (TWDP) distributions, among which the Ricean distribution had the most extensive applicability for describing small-scale fading characteristics in most indoor cases [16]. Furthermore, unified probability density function (PDF) formulas for characterizing a wide range of small-scale fading distributions were derived in [17], [18].

In this paper, we investigate the small-scale spatial fading and autocorrelation behavior of the received signal voltage amplitude for both directional and omnidirectional antenna patterns in an urban microcell (UMi) environment for both line-of-sight (LOS) and non-line-of-sight (NLOS) conditions, based on a set of outdoor measurements conducted in downtown Brooklyn, New York, using a stationary 35.31-cm (about 87 wavelengths at 73.5 GHz) linear track at the receiver to move the directional antenna, with a carrier frequency of 73.5 GHz and a radio frequency (RF) bandwidth of 1 GHz.

II. 73 GHz SMALL-SCALE FADING MEASUREMENTS

A. Measurement Hardware

The small-scale measurement campaign was conducted with a wideband sliding correlator channel sounder that transmitted at a center frequency of 73.5 GHz [19], [20]. The sounding sequence at the transmitter (TX) was a pseudorandom noise (PN) sequence of length 2047 and was generated with a field-programmable-gate-array (FPGA) and high-speed digital-to-analog converter (DAC) at a rate of 500 Megachips-per-second (Mcps) [21]. The baseband sequence was mixed with a 5.625 GHz intermediate-frequency (IF) and then upconverted with a

Sponsorship for this work was provided by the NYU WIRELESS Industrial Affiliates program and NSF research grants 1320472, 1302336, and 1555332. The authors thank Yunchou Xing, Jeton Koka, Ruichen Wang, and Dian Yu for their help in conducting the measurements.

67.875 GHz local oscillator (LO) to reach a center RF of 73.5 GHz [22]. The 1 GHz RF null-to-null bandwidth signal centered at 73.5 GHz was then transmitted through a steerable high-gain pyramidal horn antenna with 27 dBi gain and 7° azimuth and elevation half-power beamwidth (HPBW) that was elevated to a height of 4 m above ground.

At the receiver (RX), the received signal was captured with a steerable widebeam horn antenna at a height of 1.4 m with 9.1 dBi gain and 60° HPBW in the azimuth and elevation planes. The wideband RF signal was then downconverted with a 67.875 GHz LO and then further demodulated with a 5.625 GHz IF into its in-phase (I) and quadrature-phase (Q) baseband voltage signals, typical of a super-heterodyne architecture. The I and Q voltage signals were then amplified and correlated in analog with a signal identical to the TX PN sequence, but at a slightly offset rate of 499.9375 Mcps. This sliding correlation method resulted in a slide factor of 8 000, also known as the time dilation factor [23]. After the analog correlation, the I and Q channel correlated voltages were sampled with a high-speed oscilloscope and then squared and summed together ($I^2 + Q^2$) in software to result in the recorded power delay profile (PDP). For recording PDPs at various angles, the TX and RX antennas were rotated by FLIR gimbals with LabVIEW software [20]. Similarly, the RX antenna was translated in linear directions along a track controlled by LabVIEW software [21], [24]. Other specifications about the measurement hardware are detailed in Table I.

B. Measurement Environment and Procedure

The small-scale linear track measurements at 73 GHz were performed on the campus of NYU Tandon School of Engineering, representative of a UMi environment. The measurement environment is detailed in Fig. 1 with illustrations of the TX and RX locations. One TX location with the antenna height set to 4.0 m above the ground and two RX locations with the antenna height set to 1.4 m were selected to perform the measurements, where one RX was LOS to the TX while the other was NLOS. The TX was placed near the southwest corner of the Dibner library building (north and center in Fig. 1), the LOS RX was located 79.9 m away from the TX, and the NLOS RX was shadowed by the southeast corner of a building (Rogers Hall on the map) with a T-R separation distance of 75.0 m.

A stationary 35.31-cm (about 87 wavelengths at 73.5 GHz) linear track was used at each RX location in the measurements (as shown in Fig. 2), over which the RX antenna was linearly-moved in increments of half-wavelength (2.04 mm) for 175 track positions. Two orientations of the linear track were tested in the measurements: orthogonal and parallel to the initial RX antenna azimuth pointing angle. For each track orientation, six sets of small-scale fading measurements were performed, where the elevation angle of the RX antenna remained fixed at 0° (parallel to horizon) with a different azimuth angle fixed for each set of the measurements where the adjacent azimuth angles were separated by 60° (HPBW increments), such that the RX antenna swept over the entire azimuth plane after rotating through the six pointing angles. The TX antenna elevation angle was always fixed at 0° (parallel to horizon). Under the LOS condition, the TX antenna was pointed at 90° in the azimuth plane, directly towards the RX location; for NLOS, the TX antenna azimuth pointing angle was 200° , roughly towards the southeast corner of Rogers Hall in Fig. 1.

As a comparison, the 28 GHz small scale measurements

TABLE I. HARDWARE SPECIFICATIONS OF SMALL-SCALE FADING AND CORRELATION MEASUREMENTS

Description	Specification
Broadcast Sequence	11^{th} order PN Code ($L = 2^{11} - 1 = 2047$)
TX and RX Antenna Type	Rotatable Pyramidal Horn Antenna
TX Chip Rate	500 Mcps
RX Chip Rate	499.9375 Mcps
Slide Factor γ	8 000
RF Null-to-Null Bandwidth	1 GHz
PDP Threshold	20 dB down from max peak
TX/RX Intermediate Frequency	5.625 GHz
TX/RX Local Oscillator	67.875 GHz (22.625 GHz \times 3)
Carrier Frequency	73.5 GHz
TX Power	14.2 dBm
TX Antenna Gain	27 dBi
TX Azimuth/Elevation HPBW	$7^\circ/7^\circ$
EIRP	41.2 dBm
TX Heights	4.0 m
RX Antenna Gain	9.1 dBi
RX Azimuth/Elevation HPBW	$60^\circ/60^\circ$
TX-RX Antenna Polarization	V-V (Vertical-to-Vertical)
RX Heights	1.4 m
Maximum Measurable Path Loss	168 dB

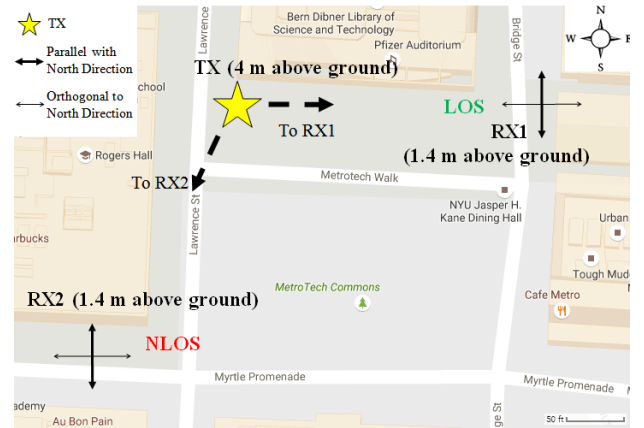


Fig. 1. 2D map depicting the small-scale measurement environment and the TX and RX locations.

presented in [25] investigated the small scale fading and autocorrelation of *individual multipath* voltage amplitudes using a 30° Az./El. HPBW RX antenna, whereas this paper studies 73 GHz fading and autocorrelation using a wider HPBW (60°) RX antenna, and focuses on received signal voltage amplitude by integrating the area under the *entire PDP* curve and then taking the square root of the total power, instead of individual multipath voltage amplitude.

C. Data Post-Processing

The processing gain incurred by sliding correlation and amplifiers in the measurement system was extracted in post-

processing for each individual PDP. A double-threshold — 20 dB down from the maximum peak and 5 dB up from the mean noise floor — was applied to each PDP to ensure signal integrity by excluding random noise spikes and low signal-to-noise ratio (SNR) artifacts. In this work, small-scale statistics for the directional measurements are meant for the amplitude of the received signal by taking the square root of the total received power in the linear scale obtained as the integral of the *entire PDP*, instead of for individual *multipath components*. The total received power for each PDP from directional measurements was determined by summing up the total power (above the threshold) under the PDP curve in the linear scale. The approximated omnidirectional received power was synthesized from directional measurements using the approach presented in [26], and was named omnidirectional received power. Although the RX antenna did not sweep the entire 4π Steradian sphere but just the azimuth plane spanning $\pm 30^\circ$ elevation coverage with respect to the horizon, a majority of the arriving energy was captured as verified in [26].

III. OMNIDIRECTIONAL SMALL-SCALE SPATIAL STATISTICS

As described above, a rotatable directive horn antenna was used at the RX side to obtain directional PDPs in the small-scale spatial fading and autocorrelation measurements. In channel modeling, however, omnidirectional statistics are usually preferred, since arbitrary antenna patterns can be implemented according to one's own needs based on the omnidirectional channel model. Therefore, in this section, we investigate small-scale spatial fading and autocorrelation of the received signal voltage amplitude for the omnidirectional RX antenna pattern [26], based on the measured data at the 73 GHz band.

A. Omnidirectional Small-Scale Spatial Fading

Fig. 3 illustrates the cumulative distribution function (CDF) of the measured small-scale spatial fading of the received signal voltage amplitude, relative to the mean value for the omnidirectional RX antenna pattern in the LOS environment, where the track orientation is orthogonal to the direct line connecting the TX and RX. Superimposed with the measured curve are the CDFs of the Rayleigh distribution, the zero-mean log-normal distribution with a standard deviation of 0.91 dB (obtained from the measured data), and the Ricean distribution with a K -factor

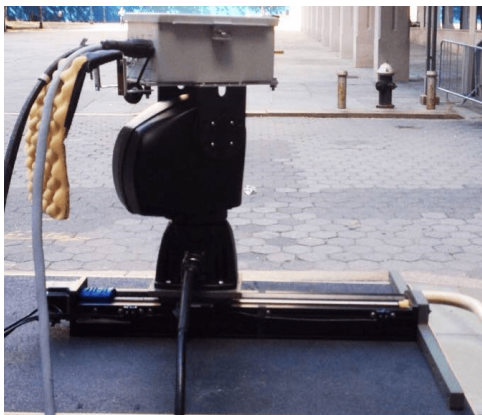


Fig. 2. The 35.31-cm (about 87 wavelengths) linear track used in the 73 GHz small-scale spatial fading and correlation measurements.

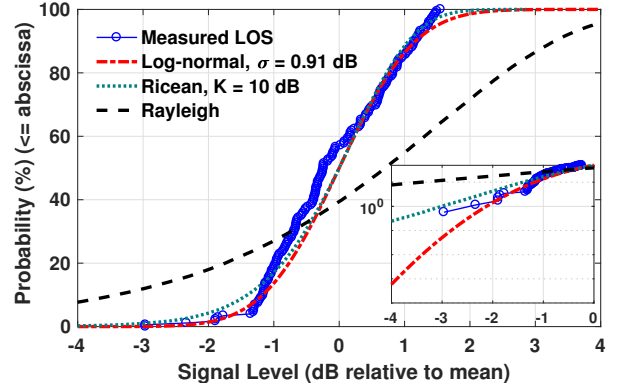


Fig. 3. CDF of the measured 73 GHz broadband small-scale spatial fading distribution of the received signal voltage amplitude over a 35.31-cm (about 87 wavelengths) linear track for the omnidirectional RX antenna pattern in the LOS environment.

of 10 dB obtained from the measured data by dividing the total received power contained in the LOS path by the power contributed from all the other reflected or scattered paths. As shown by Fig. 3, the measured 73 GHz small-scale spatial fading in the LOS environment can be approximated by the Ricean distribution with a K -factor of 10 dB, indicating that there is a dominant path (i.e., the LOS path) contributing to the total received power, and that the received signal voltage amplitude varies little over the 35.31-cm (about 87 wavelengths) length track. The log-normal distribution does not fit the measured data well in the regions of -3 to -2.5 dB and 1.2 to 1.5 dB about the mean. The maximum fluctuation of the received signal voltage amplitude is merely 3 dB relative to the mean value, whereas Rayleigh distributed fades are much deeper. The physical reason for the tiny fluctuation of the received signal voltage amplitude about the mean level in the LOS environment can be attributed to the presence of a dominant LOS path.

Small-scale spatial fading in the NLOS environment for the omnidirectional RX antenna pattern with the RX antenna translating from south to north is depicted in Fig. 4, and the zero-mean log-normal distribution with a standard deviation of 0.65 dB (obtained from the measured data) is selected to fit the measured result, and Ricean and Rayleigh distributions are also given as a reference. As evident from Fig. 4, the measured NLOS small-scale spatial fading distribution matches the log-normal fitted curve almost perfectly. In contrast, the Ricean distribution with $K = 19$ dB does not fit the measured data as well as the log-normal distribution in the tail region around -0.6 dB to -0.8 dB of relative signal level (as shown by the inset in Fig. 4), since the Ricean $K = 19$ dB distribution predicts more occurrences of deeper fading events, whereas the log-normal distribution with a 0.65 dB standard deviation predicts a more compressed fading range of -0.8 dB to 0.8 dB about the mean, which was observed for the wideband NLOS signals. The fact that the local fading of received signal voltage amplitudes in the NLOS environment is log-normal instead of Rayleigh or Ricean is similar to models in [11] for indoor factory channels. It is noteworthy that the standard deviation is only 0.65 dB, which is small and indicates minimal fluctuation in the received signal level. For the NLOS environment, there may not be a dominant path, yet the transmitted broadband signal experiences frequency-selective fading (which happens when the signal bandwidth is larger than the coherence bandwidth of

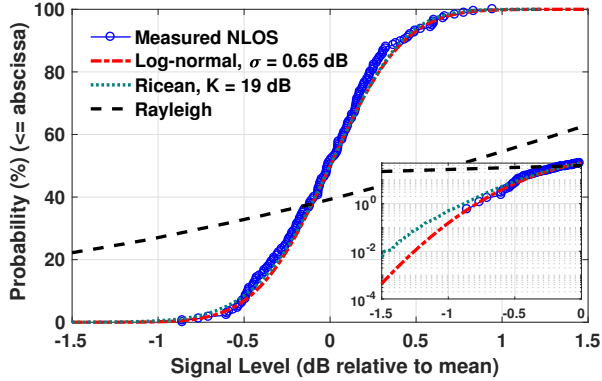


Fig. 4. CDF of the measured 73 GHz broadband small-scale spatial fading distribution of the received signal voltage amplitude over a 35.31-cm (about 87 wavelengths) linear track for the omnidirectional RX antenna pattern in the NLOS environment.

the channel), different frequency components of the signal hence experience uncorrelated fading, thus it is highly unlikely that all parts of the signal will simultaneously experience a deep fade. As a consequence, the total received power (and thus voltage amplitude) does not vary significantly over a small-scale local area. This is a distinguishing feature of the wideband signal compared to its narrowband counterpart, and also echoes the work in [13] and [14] which showed how the fading depths became smaller as the signal bandwidth increased.

B. Omnidirectional Small-Scale Spatial Autocorrelation

Apart from small-scale spatial fading, small-scale spatial autocorrelation is also a relevant research topic. Spatial autocorrelation is a metric to characterize the autocorrelation of the voltage amplitudes of the received signals across uniformly separated track positions. Spatial autocorrelation coefficient functions can be calculated using Eq. (1), where X_k denotes the k^{th} linear track position, $E[\cdot]$ is the expectation operator where the expectation is taken over all the positions X_k , and ΔX represents the spacing between different antenna positions on the track.

The measured 73 GHz wideband spatial autocorrelation coefficients of the received signal voltage amplitudes in LOS and NLOS conditions with the RX antenna moving from south to north are depicted in Fig. 5 and Fig. 6, respectively. Note that a total of 175 linear track positions were measured during the measurements, yielding a maximum spatial separation of 174 half-wavelengths. Only up to 30 wavelengths, however, are shown herein because little change is found thereafter and it provides at least 100 autocorrelation data points for all spatial separations on a single track, thus improving reliability of the statistics. Per Fig. 5, the received omnidirectional signal voltage amplitude first becomes uncorrelated at a spatial separation of about 3.5λ (where λ represents the wavelength), then becomes slightly anticorrelated for separations of 3.5λ to 10λ , and becomes slightly correlated for separations between 10λ and 18λ , and decays towards 0 sinusoidally after 18λ . Therefore, the spatial autocorrelation can be modeled by a “damped oscillation” function of (2) [27]

$$f(\Delta X) = \cos(a\Delta X)e^{-b\Delta X} \quad (2)$$

where ΔX denotes the space between antenna positions, a is an oscillation distance with units of radians/ λ (wavelength),

TABLE II. SPATIAL CORRELATION MODEL PARAMETERS IN (2) FOR 73 GHZ, 1 GHz RF BANDWIDTH ($\lambda=0.41$ CM) BASED ON THE FITTED CURVES ON MEASURED DATA OVER A 35.31-CM (ABOUT 87 WAVELENGTHS) LINEAR TRACK.

Condition	a (rad/ λ)	$T = 2\pi/a$	b (λ^{-1})	$d = 1/b$
LOS Omnidirectional	0.45	14.0λ (5.71 cm)	0.10	10.0λ (4.08 cm)
NLOS Omnidirectional	0	-	0.26	3.85λ (1.57 cm)
LOS Directional	0 - 0.50	$12.6\lambda - \infty$ (5.14 cm - ∞)	0.005 - 0.195	$5.13\lambda - 200\lambda$ (2.09 cm - 81.6 cm)
NLOS Directional	0	-	0.04 - 1.49	$0.67\lambda - 25.0\lambda$ (0.27 cm - 10.2 cm)

$T = 2\pi/a$ can be defined as the spatial oscillation period with units of λ or cm, and b is a spatial decay constant with units of λ^{-1} whose inverse $d = 1/b$ is the decorrelation distance with units of λ . a and b are obtained using the minimum mean square error (MMSE) method to find the best fit between the empirical spatial autocorrelation curve and theoretical model given by (2). The “damped oscillation” pattern can be explained by superposition of multipath components with different phases at different linear track positions. As the separation distance of linear track positions increases, the phase differences among individual multipath components will oscillate as the separation distance of track positions increases due to alternating constructive and destructive combining of the multipath phases. This “damped oscillation” pattern is obvious in LOS environment where phase difference among individual multipath component is not affected by shadowing effects that occurred in NLOS environments. The form of (2) also guarantees that the spatial autocorrelation coefficient is always 1 for $\Delta X = 0$, and converges to 0 when ΔX approximates infinity.

The spatial autocorrelation curve for NLOS environment in Fig. 6 exhibits a different trend from that in Fig. 5, which is more akin to an exponential distribution without damping, but can still be fitted using Eq. (2) with a set to 0. The constants a, b , are provided in Table II, where T is the spatial oscillation period, and d represents the spatial decay constant. From Fig. 6 and Table II it is clear that after 1.57 cm (3.85 wavelengths at 73.5 GHz) in the NLOS environment, the received voltage amplitudes become uncorrelated (the correlation coefficient decreases to $1/e$ [6]). We note that Samimi [25] found *individual multipath* voltage amplitudes in the directional measurements using a 30° Az./El. HPBW antenna became uncorrelated at physical distances of 0.52 cm (0.48 wavelengths at 28 GHz) and 0.67 cm (0.62 wavelengths at 28 GHz) in LOS and NLOS environments, respectively, whose decorrelation distances were smaller as compared to the *total received voltage* (square root of area under the PDP) at 73 GHz using a 60° Az./El. HPBW antenna for both the directional antenna pattern and synthesized omnidirectional antenna pattern.

IV. DIRECTIONAL SMALL-SCALE SPATIAL STATISTICS

This section is dedicated to the small-scale spatial fading and autocorrelation of the received signal voltage amplitudes associated with the directional RX antenna pattern.

$$\rho = \frac{E[(A_k(X_k) - \overline{A_k(X_k)})(A_k(X_k + \Delta X) - \overline{A_k(X_k + \Delta X)})]}{\sqrt{E[(A_k(X_k) - \overline{A_k(X_k)})^2]E[(A_k(X_k + \Delta X) - \overline{A_k(X_k + \Delta X)})^2]}} \quad (1)$$

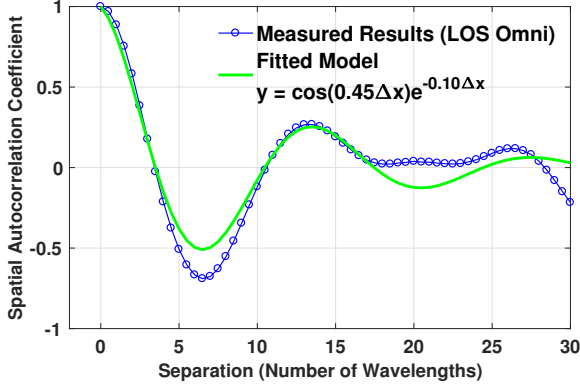


Fig. 5. Measured 73 GHz wideband spatial autocorrelation coefficients of the received signal voltage amplitude over a 35.31-cm (about 87 wavelengths) linear track for the omnidirectional RX antenna pattern in the LOS environment, and the corresponding fitted model.

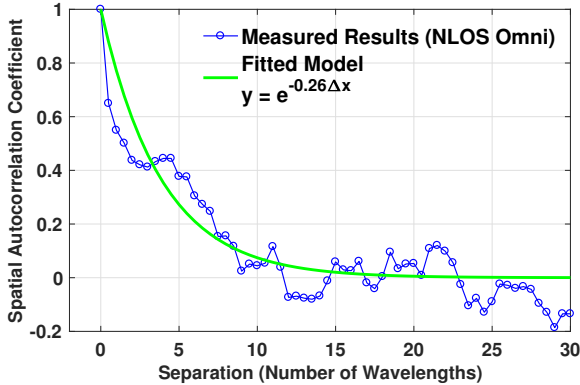


Fig. 6. Measured 73 GHz wideband spatial autocorrelation coefficients of the received signal voltage amplitude over a 35.31-cm (about 87 wavelengths) linear track for the omnidirectional RX antenna pattern in the NLOS environment, and the corresponding fitted model.

A. Directional Small-Scale Spatial Fading

The small-scale spatial fading of the received signal voltage amplitudes along the linear track using the 7° azimuth and elevation HPBW TX antenna and 60° HPBW RX antenna with the RX antenna translating from south to north in LOS and NLOS conditions are drawn in Fig. 7 and Fig. 8, respectively, where each measured curve corresponds to a unique RX antenna azimuth pointing angle as specified in the legend. Note that there was no signal for the RX azimuth pointing angle of 270° in the NLOS environment, thus the corresponding results are absent in Fig. 8. As is observed from Figs. 7 and 8, the CDFs of measured directional spatial signal voltage amplitude fading resemble Ricean distributions in both LOS and NLOS environments, which are similar to the results obtained from 28 GHz small-scale fading measurements and results presented in [25]. The possible physical reason for such distributions is that only one dominant path (accompanied with several weaker paths in some cases) was obtained by the horn antenna due to its directionality (i.e., limited HPBW), and that mmWave

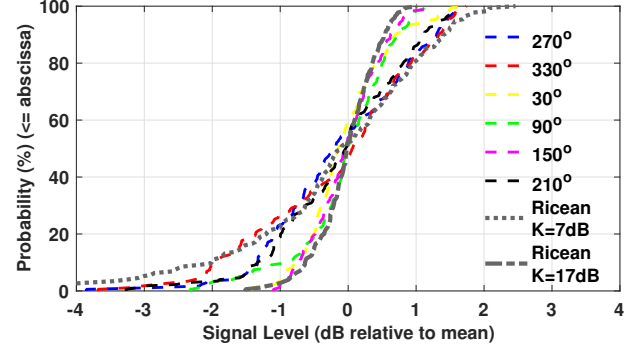


Fig. 7. Measured 73 GHz small-scale spatial fading distributions of the directional received signal voltage amplitude over a 35.31-cm (about 87 wavelengths) linear track in LOS conditions, and the corresponding Ricean fitted curves with different K -factors. The angles in the legend denote the receiver antenna azimuth pointing angle during the small-scale measurements with 270° denoting the angle pointing directly at the transmitter.

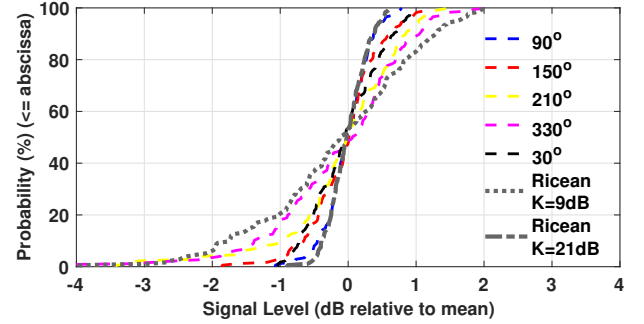


Fig. 8. Measured 73 GHz small-scale spatial fading distributions of the directional received signal voltage amplitude over a 35.31-cm (about 87 wavelengths) linear track in NLOS conditions, and the corresponding Ricean fitted curves with different K -factors. The angles in the legend denote the receiver antenna azimuth pointing angle during the small-scale measurements with 30° denoting the angle pointing roughly directly at the transmitter.

propagation is directional and the channel is sparse. The Ricean K -factor ranges from 7 dB to 17 dB for LOS conditions, and 9 dB to 21 dB for NLOS cases, as shown in Figs. 7 and 8. The comparable Ricean K -factors in LOS and NLOS environments indicate that the environment (LOS or NLOS) does not influence the Ricean fading, namely, for a directional RX antenna in either LOS or NLOS environment, there exists a dominant path whose power is much higher than the other weaker paths, and the power ratio of the dominant path to weaker paths is similar in LOS and NLOS environments in mmWave channels.

B. Directional Small-Scale Spatial Autocorrelation

Figs. 9 illustrates the spatial autocorrelation coefficients of the received signal voltage amplitudes versus RX antenna separation for individual antenna pointing angles in the LOS environment, where the RX antenna was moved in an orthogonal manner relative to the T-R line. The angles in the legend denote the RX antenna azimuth pointing angles relative to true north. As shown by Fig. 9, all of the six spatial autocorrelation

curves in the LOS environment exhibit sinusoidally exponential decaying trends (albeit with different oscillation and decay rates), which is similar to the omnidirectional case displayed in Fig. 5.

The spatial autocorrelation curves for the RX antenna translations parallel with respect to the T-R line are illustrated in Fig. 10 (since there were random pedestrians blocking the RX antenna when the RX antenna pointed at 30° , the corresponding result was biased hence not plotted). It is intriguing to observe that the autocorrelations do not always follow the sinusoidal-exponential function as in Fig. 9. For the RX antenna pointing angle of 270° , for instance, the received signal voltage amplitude is highly correlated with a slowly-decaying autocorrelation curve, which can be physically interpreted by the fact that the TX and RX antennas were always directly pointing at each other while the RX antenna moved along the track, thus only a LOS path was received whose amplitude varied gradually with the minor changes in the T-R separation distance. In contrast, the autocorrelation function drops quickly from 1 to 0 and becomes increasingly negative as the antenna separation increases for the RX antenna pointing angles of 330° and 210° , for which the RX antenna was pointing towards a building and a grove area, respectively, and there was only one resolvable multipath component in the PDP. The spatial decorrelation distance $d = 1/b$ using model (2) is found to be 200 wavelengths, which is an "extrapolation" of the sinusoidal model, meaning that the correlation drops to $1/e$ at 200 wavelengths and is always below $1/e$ afterwards.

For the NLOS environment, the spatial autocorrelation coefficients of the received signal voltage amplitudes for individual antenna pointing angles for one antenna translation direction are plotted in Fig. 11 (the results for the other track orientation are very similar to the ones shown here), wherein the results for the majority of the RX pointing angles are in line with that given by Fig. 6, which follow the exponential function and agree well with the 28 GHz NLOS small-scale spatial autocorrelation coefficients of multipath voltage amplitudes described in [25]. One exception is the 30° pointing angle, where the autocorrelation coefficient slowly decreases from 1 to 0.2 or so, probably due to the presence of a dominant path with a relatively constant signal level, which may be caused by the diffraction of the southeast corner of Rogers Hall in Fig. 1.

The spatial autocorrelation model parameters in (2), along with the spatial oscillation period T and spatial decay constant d , are summarized in Table II for both omnidirectional and directional RX antenna patterns under LOS and NLOS environments. For the LOS environment, the decorrelation distance ranges from around five wavelengths to 200 wavelengths (2.09 - 81.6 cm), while the NLOS decorrelation distance is between 0.67 and 25 wavelengths at 73.5 GHz (0.27 - 10.2 cm) at 73.5 GHz. The 200-wavelength decorrelation distance is calculated/predicted using the model in (2) based upon the measured data over a track length of 30 wavelengths, which corresponds to the 210° and 330° curves in Fig 10, in which case the RX antenna was pointing at a main reflector and there was only one resolvable multipath component in the PDP (with a 20 dB down threshold [6]). The 200-wavelength decorrelation distance means that the correlation is smaller than $1/e$ after 200 wavelengths, but the correlation may also be less than $1/e$ at some points, and increases and decreases in a sinusoidal manner within 200 wavelengths. The above observations indicates that

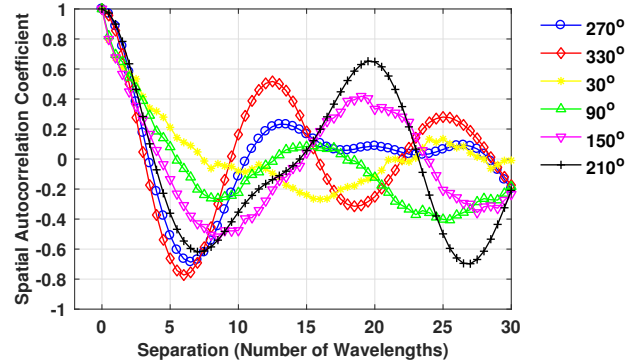


Fig. 9. Measured 73 GHz spatial autocorrelation coefficients of the directional received signal voltage amplitude over a 35.31-cm (about 87 wavelengths) linear track in the LOS environment with the RX antenna translating orthogonally relative to the T-R line. The angles in the legend denote the receiver antenna azimuth pointing angle during the small-scale measurements with 270° denoting the angle pointing directly at the transmitter.

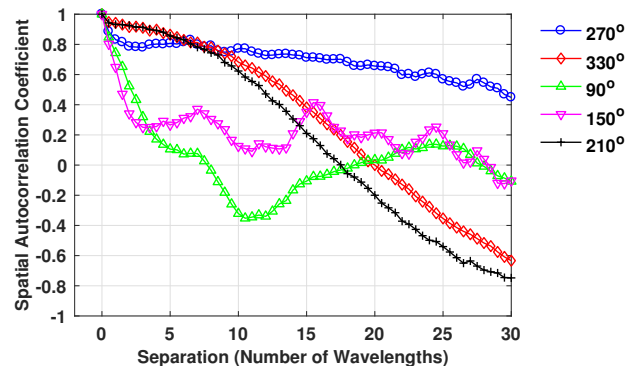


Fig. 10. Measured 73 GHz spatial autocorrelation coefficients of the directional received signal voltage amplitude over a 35.31-cm (about 87 wavelengths) linear track in the LOS environment with the RX antenna translating in a parallel manner with respect to the T-R line. The angles in the legend denote the receiver antenna azimuth pointing angle during the small-scale measurements with 270° denoting the angle pointing directly at the transmitter.

the decorrelation distance is the largest when the RX antenna points at a major reflector and moves in a parallel manner with respect to the T-R line, and the smallest decorrelation distance occurs when the RX antenna is pointing roughly to the opposite direction of the TX and without major reflectors. These decorrelation distances are valuable to antenna design [28].

V. CONCLUSION

This paper has investigated the wideband small-scale spatial fading and autocorrelation of the received signal voltage amplitudes at 73 GHz, for both omnidirectional and directional receiver antenna patterns in both LOS and NLOS environments in a UMi scenario.

When measured over a 35.31-cm (about 87 wavelengths) linear track, for the omnidirectional antenna pattern, the LOS fading obey the Ricean distribution with a K -factor of 10 dB, while the NLOS fading can be described by the log-normal distribution with a standard deviation of 0.65 dB. The fading depth ranges from -3 dB to 1.5 dB relative to the mean for LOS, and -0.8 dB to 0.8 dB for NLOS. For the directional antenna pattern, fading in both LOS and NLOS environments follows the Ricean distribution, where the K -factor ranges from 7 dB to 17 dB for LOS, and 9 dB to 21 dB for NLOS. and the fading

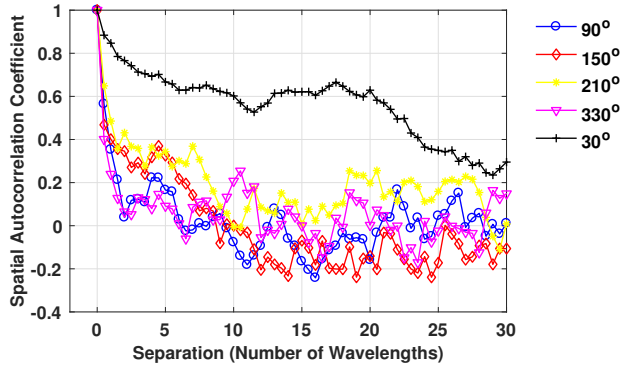


Fig. 11. Measured 73 GHz spatial autocorrelation coefficients of the directional received signal voltage amplitude over a 35.31-cm (about 87 wavelengths) linear track in the NLOS environment. The angles in the legend denote the receiver antenna azimuth pointing angle during the small-scale measurements with 30° denoting the angle pointing roughly directly at the transmitter.

depth varies between -4 dB to 2 dB for both LOS and NLOS environments.

In terms of the spatial autocorrelation of received signal voltage amplitudes, it follows the sinusoidal-exponential distribution in the LOS environment for the omnidirectional RX antenna and most directional antenna cases, and the exponential distribution for directional RX antenna when the RX antenna moves in a parallel manner with respect to the T-R line. In the NLOS environment, the spatial autocorrelation can be modeled by the exponential distribution for both omnidirectional and directional RX antennas. For the LOS environment, the decorrelation distance ranges from around five wavelengths to 200 wavelengths (2.09 - 81.6 cm), while the NLOS decorrelation distance is between 0.67 and 25 wavelengths (0.27 - 10.2 cm) at 73.5 GHz. It gives rise to the maximum decorrelation distance when the RX antenna points at a major reflector and moves in a parallel manner with respect to the T-R line, while the minimum decorrelation distance is likely to occur when the RX antenna is pointing roughly to the opposite direction of the TX and without major reflectors. The short correlation distance in most cases is favorable for spatial multiplexing in MIMO, since it allows for uncorrelated spatial data streams to be transmitted from closely-spaced (a fraction to several wavelengths) antennas.

REFERENCES

- [1] T. S. Rappaport *et al.*, *Millimeter Wave Wireless Communications*. Pearson/Prentice Hall 2015.
- [2] —, “Millimeter wave mobile communications for 5G cellular: It will work!” *IEEE Access*, vol. 1, pp. 335–349, 2013.
- [3] —, “Wideband millimeter-wave propagation measurements and channel models for future wireless communication system design,” *IEEE Transactions on Communications*, vol. 63, no. 9, pp. 3029–3056, Sept. 2015.
- [4] A. Ghosh *et al.*, “Millimeter-wave enhanced local area systems: A high-data-rate approach for future wireless networks,” *IEEE Journal on Selected Areas in Communications*, vol. 32, no. 6, pp. 1152–1163, June 2014.
- [5] G. R. MacCartney *et al.*, “Indoor office wideband millimeter-wave propagation measurements and channel models at 28 and 73 GHz for ultra-dense 5G wireless networks,” *IEEE Access*, vol. 3, pp. 2388–2424, 2015.
- [6] M. K. Samimi and T. S. Rappaport, “3-D millimeter-wave statistical channel model for 5G wireless system design,” *IEEE Transactions on Microwave Theory and Techniques*, vol. 64, no. 7, pp. 2207–2225, July 2016.
- [7] K. Haneda *et al.*, “5G 3GPP-like channel models for outdoor urban micro-cellular and macrocellular environments,” in *2016 IEEE 83rd Vehicular Technology Conference (VTC Spring)*, May 2016, pp. 1–7.
- [8] R. Bultitude, “Measurement, characterization and modeling of indoor 800/900 MHz radio channels for digital communications,” *IEEE Communications Magazine*, vol. 25, no. 6, pp. 5–12, June 1987.
- [9] Q. Wang *et al.*, “Ray-based analysis of small-scale fading for indoor corridor scenarios at 15 GHz,” in *2015 Asia-Pacific Symposium on Electromagnetic Compatibility (APEMC)*, May 2015, pp. 181–184.
- [10] E. Tanghe *et al.*, “Statistical modelling of power delay profiles and small-scale fading in industrial environments,” in *2009 IEEE Antennas and Propagation Society International Symposium*, June 2009, pp. 1–4.
- [11] T. S. Rappaport *et al.*, “Statistical channel impulse response models for factory and open plan building radio communication system design,” *IEEE Transactions on Communications*, vol. 39, no. 5, pp. 794–807, May 1991.
- [12] W. Q. Malik *et al.*, “Impact of bandwidth on small-scale fade depth,” in *IEEE GLOBECOM 2007 - IEEE Global Telecommunications Conference*, Nov. 2007, pp. 3837–3841.
- [13] J. M. Holtzman and L. M. A. Jalloul, “Rayleigh fading effect reduction with wideband DS/CDMA signals,” *IEEE Transactions on Communications*, vol. 42, no. 234, pp. 1012–1016, Feb 1994.
- [14] G. D. Durgin and T. S. Rappaport, “Theory of multipath shape factors for small-scale fading wireless channels,” *IEEE Transactions on Antennas and Propagation*, vol. 48, no. 5, pp. 682–693, May 2000.
- [15] G. Durgin and T. S. Rappaport, “Basic relationship between multipath angular spread and narrowband fading in wireless channels,” *Electronics Letters*, vol. 34, no. 25, pp. 2431–2432, Dec 1998.
- [16] A. H. Henderson *et al.*, “Finding the right small-scale fading distribution for a measured indoor 2.4 GHz channel,” in *2008 IEEE Antennas and Propagation Society International Symposium*, July 2008, pp. 1–4.
- [17] Y. Sun *et al.*, “Corrections to Unified Laguerre Polynomial-Series-Based Distribution of Small-Scale Fading Envelopes,” *IEEE Transactions on Vehicular Technology*, vol. 60, no. 1, pp. 347–349, Jan. 2011.
- [18] C. C. Chai and T. T. Tjhung, “Unified laguerre polynomial-series-based distribution of small-scale fading envelopes,” *IEEE Transactions on Vehicular Technology*, vol. 58, no. 8, pp. 3988–3999, 2009.
- [19] D. Cox, “Delay doppler characteristics of multipath propagation at 910 MHz in a suburban mobile radio environment,” *IEEE Transactions on Antennas and Propagation*, vol. 20, no. 5, pp. 625–635, Sept. 1972.
- [20] G. R. MacCartney, Jr. and T. S. Rappaport, “73 GHz millimeter wave propagation measurements for outdoor urban mobile and backhaul communications in New York City,” in *2014 IEEE International Conference on Communications (ICC)*, June 2014, pp. 4862–4867.
- [21] G. R. MacCartney, Jr. *et al.*, “Millimeter-wave human blockage at 73 GHz with a simple double knife-edge diffraction model and extension for directional antennas,” in *2014 IEEE 84th Vehicular Technology Conference (VTC2016-Fall)*, Sept. 2016.
- [22] —, “Millimeter wave wireless communications: New results for rural connectivity,” in *All Things Cellular’16: Workshop on All Things Cellular Proceedings, in conjunction with ACM MobiCom*, Oct. 2016.
- [23] T. S. Rappaport, *Wireless Communications: Principles and Practice*, 2nd ed. Upper Saddle River, NJ: Prentice Hall, 2002, ch. 5.
- [24] S. Deng *et al.*, “Indoor and outdoor 5G diffraction measurements and models at 10, 20, and 26 GHz,” in *2016 IEEE Global Telecommunications Conference (GLOBECOM)*, Dec. 2016.
- [25] M. K. Samimi *et al.*, “28 GHz millimeter-wave ultrawideband small-scale fading models in wireless channels,” in *2016 IEEE 83rd Vehicular Technology Conference (VTC 2016-Spring)*, May 2016, pp. 1–6.
- [26] S. Sun *et al.*, “Synthesizing omnidirectional antenna patterns, received power and path loss from directional antennas for 5G millimeter-wave communications,” in *2015 IEEE Global Communications Conference (GLOBECOM)*, Dec. 2015, pp. 1–7.
- [27] Y. Zhang *et al.*, “A novel spatial autocorrelation model of shadow fading in urban macro environments,” in *2008 IEEE Global Telecommunications Conference (GLOBECOM)*, Nov 2008, pp. 1–5.
- [28] R. B. Ertel *et al.*, “Overview of spatial channel models for antenna array communication systems,” *IEEE Personal Communications*, vol. 5, no. 1, pp. 10–22, Feb 1998.